

Simulating a discrete time crystal over 57 qubits on a quantum computer

Philipp Frey and Stephan Rachel

School of Physics, University of Melbourne, Parkville, VIC 3010, Australia

(Dated: March 21, 2022)

We simulate the dynamics of a spin-1/2 chain with nearest neighbor Ising interactions, quenched disorder and periodic driving over 57 qubits on a current quantum computer. A transition between time crystalline behaviour and non-symmetry breaking dynamics is observed via critical fluctuations in the sub-harmonic frequency response of the system. We probe shorter time scales by implementing the Floquet unitary directly, as well as longer time scales by making use of an equivalent Hamiltonian description. In order to extract the signal from the noisy data produced by current quantum computer devices, we develop a strategy for error mitigation and show that the results are robust under variations of the parameters introduced in this scheme. Our findings are in agreement with previous numerical simulations but add larger system size data points to the phase diagram.

I. INTRODUCTION

It is well known that the equilibrium states of some physical systems exhibit less symmetry than the underlying dynamical description might lead one to believe. That is, not every dynamical symmetry of a given system is necessarily also a symmetry of its equilibrium state. This phenomenon of spontaneous symmetry breaking is rather common in nature and used to characterise a large class of phase transitions in materials. For instance, a crystal lattice breaks the continuous spatial translation symmetry of the underlying Hamiltonian as indicated by the mere discrete translation symmetry of the local density operator. In 2012, Wilczek proposed the existence of phases of matter that break continuous time translation symmetry [1]. These so-called time crystals have since been ruled out in equilibrium for a large class of systems [2]. However, it has been shown that this type of phase can exist in Floquet systems and be stable (for reviews see [3, 4]). Here, the dynamical symmetry consists of discrete time translations only. Hence we speak of discrete time crystals (DTC). DTCs exhibit period doubling, tripling etc. with respect to the periodic driving Hamiltonian. That is, the system returns to its initial state only after some integer $n > 1$ multiple of the driving period T (see Eq. 5). DTCs have been subject of theoretical and experimental investigation in recent years [5–8]. A well studied instance is the one-dimensional spin-1/2 chain with nearest neighbour interactions and random local magnetic field strength, driven by an imperfect periodic spin flip [9–11].

One signature of the DTC phase are long-time stable oscillations of the individual spins. The time resolved two-point correlator $\langle \sigma_i^z(t) \sigma_i^z(0) \rangle$ will not approach the equilibrium value $\langle \sigma_i^z(t) \rangle \langle \sigma_i^z(0) \rangle$, indicating that the system retains memory of the initial state in violation of the eigenstate thermalization hypothesis. This implies that the DTC phase has to be many body localized (MBL). MBL has been a subject of extensive research in recent years, both theoretical and experimental [12–23]. It can be understood as an emergent integrability through localized integrals of motion. In their presence the system

is prevented from heating to a state that locally resembles thermal equilibrium. For comprehensive reviews on MBL see [24–28]. We furthermore require that $\langle \sigma_i^z(t) \rangle$ remains finite, as it is the observable that we actually measure. MBL phases without this DTC signature are therefore entirely possible. Indeed it has been shown that this particular Floquet system in the high frequency limit is unitarily equivalent to a random transverse field Ising model (TFIM) when considering even multiples of the driving period T [10]. The latter has a thermal phase and two distinct MBL phases. In one of the MBL phases the hidden Ising symmetry $\prod_i \sigma_i^x$ remains intact while in the other one it is spontaneously broken. The latter therefore corresponds to a DTC phase.

Previous research on this system is either based on numerical calculations or experiments with ultra-cold atoms [29, 30], trapped ions [9, 19] and dipolar spins [31, 32]. While exact diagonalisation [10] provides access to a wide range of observables with high precision, it is limited to rather small spin chains with on the order of 10 to 20 sites. Other numerical techniques use tensor networks such as matrix product states and are mostly restricted to ground states or short time scales [33–37]. Current noisy intermediate-scale quantum (NISQ) devices like IBM’s superconducting circuits provide up to 65 qubits at the cost of being rather noisy compared to classical computation. One therefore often has to employ some form of error mitigation in order to extract physics from raw data [38]. Nevertheless, they allow us to simulate the dynamical evolution of systems with considerably more degrees of freedom than any classical computer. Due to the limited connectivity on current devices, one is mostly restricted to one-dimensional systems with nearest neighbor interactions only. The challenge presented to us is to identify interesting physical phenomena that can be observed in principle on NISQ devices and to implement forms of error mitigation that reduce noise as much as possible. A major advantage over experimental setups is that, barring issues with high error-rates, it is relatively straightforward to implement arbitrary Hamiltonians and to adjust interactions at will once the system has

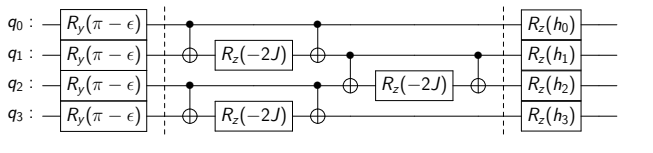


FIG. 1. Illustrative 4-qubit circuit for one Floquet-period. R_y and R_z are single-qubit rotations. Vertical lines connecting small and large open circles represent CNOT gates.

been mapped to a set of qubits. Because of its potential advantages, quantum simulation on NISQ devices has developed into an active field of research both in general [39–44] and in regards to MBL specifically [45, 46].

In this paper we make an attempt to observe a dynamical phase transition in a driven system on a current NISQ superconducting circuit device with a heavy hex topology, the 65-qubit *ibmq_manhattan*, with stated average CNOT error rates of $1.9\text{e-}2$ and average readout error rates of $3.5\text{e-}2$.

II. DTC ON A QUANTUM COMPUTER

A. Floquet system

The time evolution operator U of the Floquet-system is defined in terms of two unitaries $U = U_2 U_1$, one representing an imperfect global spin flip,

$$U_1 = \frac{\pi}{2}(1 - \epsilon) \sum_i \sigma_i^x, \quad (1)$$

and the other one nearest neighbor Ising interactions and quenched local disorder,

$$U_2 = \exp\left(-i \left[J \sum_i \sigma_i^z \sigma_{i+1}^z + B_i^z \sigma_i^z \right]\right). \quad (2)$$

The parameter ϵ accounts for a deviation from an ideal spin flip. Qualitatively novel behaviour needs to be robust against small perturbations in order to be considered a true phase of the system. The second unitary can be varied by adjusting the Ising interaction strength J , as well as the local magnetic field strength B_i^z . The latter is randomly chosen from an interval $[0, 2\pi]$ for each site independently.

We choose a completely polarized chain of spins up as the initial state. We use a trotterized time evolution, which, for this model, is an exact representation of the unitary U . In Fig. 1 we show the circuit decomposition in terms of basis gates for an Trotter step on 4 qubits. We then measure each qubit in the computational basis corresponding to σ^z . The error rates on current NISQ devices limits the number of Floquet periods to ~ 20 .

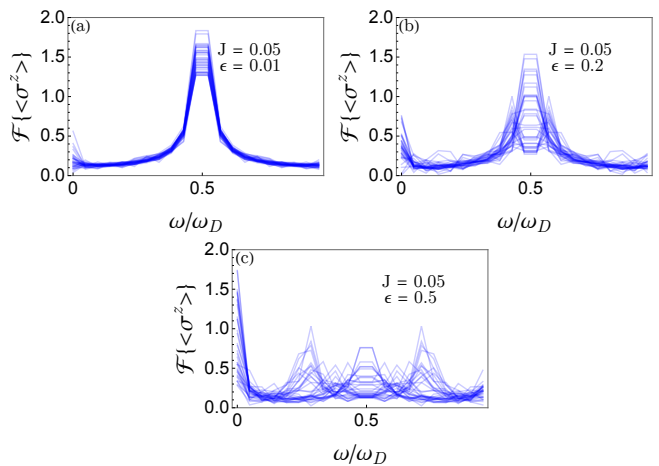


FIG. 2. Sub-harmonic frequency response of the driven Floquet system (a) for small perturbation (DTC), (b) in the transition regime, (c) for large perturbation (trivial MBL).

By making use of the topology of *ibmq_manhattan* (see Fig. 8) we are able to simulate an $N = 57$ site chain and to thereby go far beyond current numerical calculations on any classical computer. The circuit for each time step is run 8192 times in order to minimize shot noise. Following [10], we will look at several signatures of the DTC phase and the transition to the trivial MBL phase. The first one being a pronounced peak in the Fourier spectrum of $\langle \sigma_i^z(t) \rangle$ at half the driving frequency $\omega_D = 2\pi T^{-1}$ for each spin. Fig. 2 shows the discrete Fourier spectrum for fixed J and varying ϵ after applying a filter to reduce the overall noise (see Sec. III A). The sub-harmonic response at low ϵ is destroyed for large perturbations. In between we see a transition as indicated by the fact that some spins show a clear sub-harmonic peak while others do not.

This leads us to the second signature, namely critical fluctuations at the transition between the DTC and the trivial MBL phase in the order parameter that spontaneously breaks the Ising symmetry in one phase but not in the other. The order parameter of the random Ising transition is the z -magnetisation and a finite value will result in stable oscillations at $\omega = \omega_D/2$ due to the periodic flip operation. Defining $h_i = |\mathcal{F}\{\langle \sigma_i^z(t) \rangle\}(\omega_D/2)|$, with $\mathcal{F}\{\cdot\}$ representing the Fourier transform, one can conclude that the variance across the chain $\text{Var}(\{h_i\})$ should vanish in the DTC phase as well as in the trivial MBL phase. At the transition we instead expect critical fluctuations to produce a finite value. For short chains ($N \sim 10$) one has to average over several disorder realizations to obtain a clear signal since the behaviour at the transition is sensitive to the particular choice of disorder. Our system of $N = 57$ sites seems to produce a rather clear signal without this averaging process, as one might expect. Fig. 3 shows the variance as a function of ϵ for different values of J after we have reduced the noise by

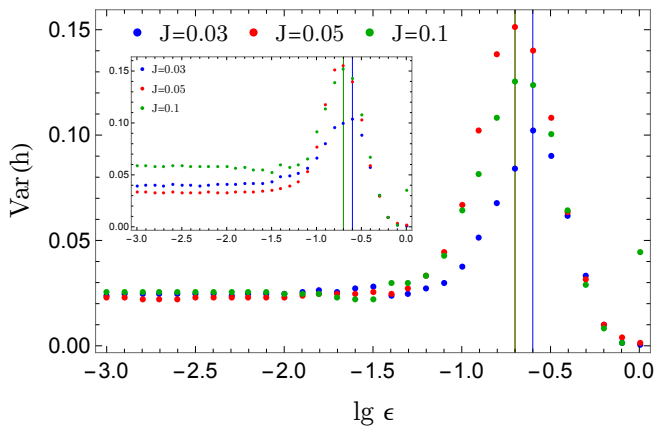


FIG. 3. Critical fluctuations at the transition between DTC and trivial MBL. Data evaluated using the least noisy 35 out of 57 qubits. Vertical lines mark the peak positions of the three curves. Inset: data evaluated with 45 qubits.

applying a selection filter (see Sec. III A). A pronounced peak indicates the phase transition and allows us to extract an estimate for the critical value of ϵ .

B. Equivalent Hamiltonian system

The issue with probing only 20 time steps is that one might merely observe initial transients instead of the true long term DTC phenomenon. It is thus essential to probe longer time scales. In order to accomplish this, we make use of the fact that for even integer time steps the Floquet model is unitarily equivalent to a Hamiltonian system [10]. For $|TB^z|, |TJ| \ll 1$:

$$V U(T) V^\dagger = e^{-iH_{\text{TFIM}}T} \prod_i \sigma_i^x, \quad (3)$$

with V a finite depth unitary operator that depends on the particular disorder and the TFIM Hamiltonian

$$H_{\text{TFIM}} = \sum_i \tilde{J}_i \sigma_i^z \sigma_{i+1}^z + \tilde{B}_i^x \sigma_i^x. \quad (4)$$

Thus one finds that

$$V U(2nT) V^\dagger = e^{-i2nH_{\text{TFIM}}T}. \quad (5)$$

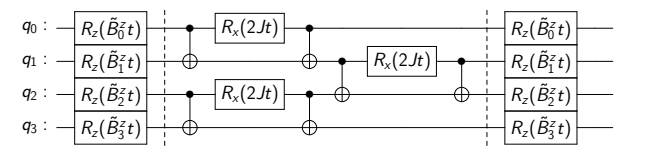


FIG. 4. 4-qubit symmetric Trotter step for the TFIM.

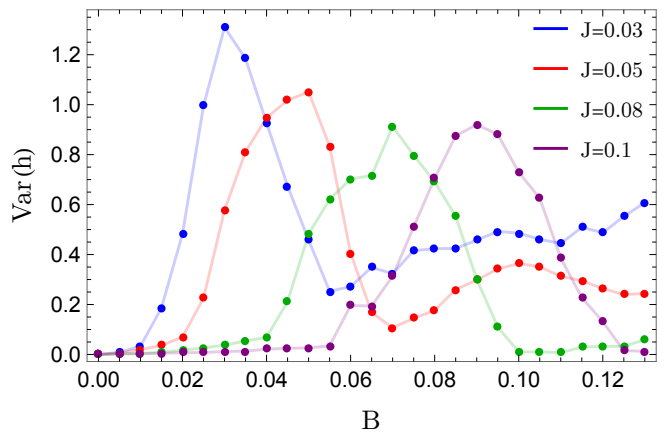


FIG. 5. Critical fluctuations at the transition in the random TFIM for different values of the spin-spin interaction strength J . Data evaluated using a threshold of $W_0 = 0.45$.

Simulating H_{TFIM} with random \tilde{J}_i^z and \tilde{B}_i^x is therefore equivalent to simulating the Floquet system if one shifts the Fourier spectrum $\mathcal{F}\{\langle\sigma_i^z(t)\rangle\}$ by $\omega_D/2$. However, the Trotter step size for this Hamiltonian system can be made larger than one unit of time in the Floquet model which allows us to approximate states at later times within a reasonable circuit depth. The transverse field \tilde{B}_i^x relates to the original ϵ through $\tilde{B}_i^x \equiv B(1 - b_i)$, with $B \sim \epsilon$ and $b_i \in [0, (TB^z)^2]$, while \tilde{J}_i^z can w.l.o.g. be taken as constant and equal to the original J . Tuning B while keeping J and the disorder strength constant should result in a phase transition as observed in the Floquet system. In order to probe later times we use five larger Trotter steps to skip over the initial transient oscillations followed by a series of ten smaller steps. The size of the larger steps is chosen based on numerical simulations for smaller chains. The validity of the high-frequency approximation was ensured by taking $\delta t = 0.1$ as the fundamental time step in these simulations. Each of the large Trotter steps corresponds to $60 \delta t$, while the smaller Trotter steps represent $10 \delta t$ each. We use a symmetric Trotter decomposition and interchange the x -axis and z -axis. This reduces the overall error rate since z -rotations are implemented in software and therefore essentially error free.

Fig. 5 shows the variance in the Fourier amplitude corresponding to the sub-harmonic frequency in the Floquet system as a function of transverse magnetic field strength. Again we see a clear peak indicating a transition, which allows us to read off an approximate value for the critical field strength. This value seems to scale with J in an approximately linear fashion.

C. Discussion

Based on the position and width of the peaks in Fig. 5 we can extract an approximate phase diagram for the small- J regime Fig. 6. The result seems to be compatible with the numerical calculations in Ref. 10. For relatively short chains one expects finite size scaling effects for the transition point. Considering $B = \epsilon$ in the high frequency limit and an additional factor of $\pi/2$ when converting our definition of ϵ to the one in Ref. 10, our results indicate that the transition line from DTC to non-symmetry breaking MBL is pushed to slightly larger values of B and ϵ as compared to Ref. 10. However, the uncertainties are currently comparable to the observed differences so that we cannot make a precise statement with regards to scaling.

III. ERROR MITIGATION

For current NISQ devices error mitigation is crucial. Notably, there has been significant progress in developing error mitigation schemes and demonstrating stability of quantum circuits against quantum gate errors and shot noise [38, 47–49]. For this paper we decided to develop a scheme based on our prior knowledge of the underlying physics.

A. Floquet system

The cumulative error for large circuit depths and quite significant measurement errors on some of the qubits result in a finite variance even in the suspected DTC phase. Given the systematic nature of these errors, one expects that the Fourier spectrum of every spin should acquire a finite contribution at $\omega = 0$ but to a varying degree. This is exactly what we observe in our data. In order to clean up the signal we omit the m most error-ridden qubits as

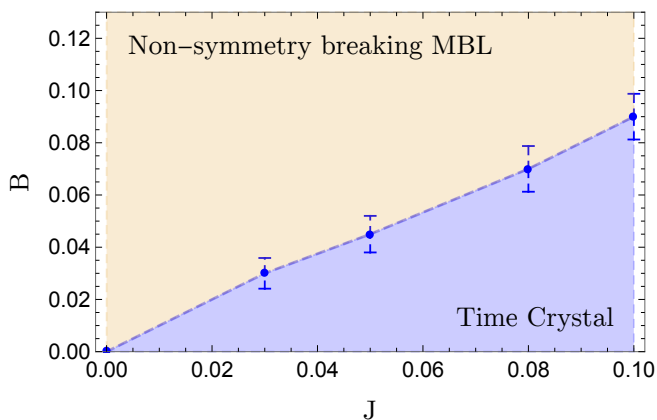


FIG. 6. Phase diagram in the small- J regime. The error bars correspond to half width half maximum of the peaks in 5.

judged by the amplitude h_i . Two different choices for m ($m = 12$ and $m = 22$) are shown in Fig. 3 to demonstrate that the signal is less clean but still present for smaller m . This might be justified by comparing simulations for short chains ($N \sim 10$) on the quantum computer to more precise classical numerics, where this effect is absent. One should note that there is a lack of consistency in the calibration and error rates of the processor since we had to collect the data over the course of several days.

B. Hamiltonian system

A further advantage of simulating the Hamiltonian system is that for a completely polarized initial state and $B = 0$ the time evolution is trivial because it is an eigenstate of the Hamiltonian. Comparison with the quantum computer allows us to estimate and compensate for the gate errors introduced in each trotter step. For $B = 0$, the random spin flip errors should result in an exponential decay of the initial polarization, which is what we observe. To compensate for this decay, we would like to rescale the data accordingly. We use the following algorithm in order to distinguish between a qubit being non-polarized at late times due to thermalization versus due to erroneous spin flips:

1. Introduce a cutoff parameter $W_0 \in [0, 1]$, where 1 corresponds to the maximal polarisation of a qubit. Qubits whose polarization drops below W_0 after the initial time evolution for $B = 0$ are excluded from the evaluation (further justification below).
2. Introduce a fixed threshold $W_f < W_0$ for finite values of B . Qubits that lie within the interval $[-W_f, W_f]$ after the initial time evolution are assumed to approach vanishing magnetization due to thermalization, in which case the accumulated gate error in the magnetisation is less significant ($\langle \sigma^z \rangle = 0$ is a fixed point as far as the Trotter gate errors are concerned). Therefore we do not rescale the subsequent data points for these qubits.
3. Qubits outside of this interval are assumed to have been outside for most of the preceding time evolution and therefore have been subject to considerable damping on the order of that observed for $B = 0$. We rescale the subsequent data points with an exponential fit obtained from the $B = 0$ data for this qubit but adjusted by the decay constant obtained for the particular value of B . With $m_i^{(B)}(t)$ denoting the magnetisation of the i 'th' qubit at time t for magnetic field B as measured on the QC, the general exponential fit takes the form

$$\frac{m_i^{(B)}(t) + 1}{2} = a_i^{(B)} e^{-b_i^{(B)} t} + c_i^{(B)}, \quad (6)$$

with fit parameters $a_i^{(B)}$, $b_i^{(B)}$ and $c_i^{(B)}$. We define the rescaled magnetisation $M_i^{(B)}(t)$ via

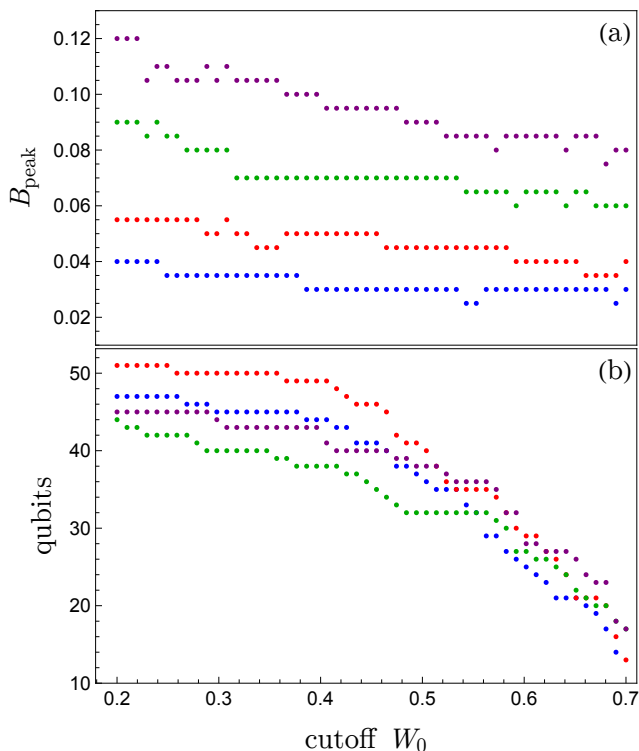


FIG. 7. (a) Peak position as a function of the cutoff W_0 . (b) Number of qubits that enter the evaluation after every filter in the error mitigation scheme has been applied.

$$M_i^{(B)}(t) = \frac{m_i^{(B)}(t) + 1}{\frac{a_i^{(0)}}{a_i^{(B)}} \left(a_i^{(B)} e^{-b_i^{(B)} t} + c_i^{(B)} \right)} - 1. \quad (7)$$

Based on numerical simulations for smaller chains one expects the individual spins to approach an almost steady state after initial, short lived transients. One therefore predicts that most spins would exhibit an exponential decay even for finite B , albeit with a different decay constant due to the modified trotter steps. Again we observe that most qubits match this prediction. By using the decay constant appropriate for finite- B time evolution we avoid overcorrection as indicated by a significant and monotonous increase in polarization over subsequent time steps, which would artificially boost the resulting signal. Our approach is therefore rather conservative. Since not all of the 57 qubits seem to operate within the margins given by the stated error rates, we additionally remove those few ones that deviate significantly from the exponential decay model as judged by convergence of our fit. The above procedure requires us to omit qubits whose error rates are sufficiently high to move their polarization into the interval $[-1, W_0]$ even for $B = 0$, because we would otherwise confuse them for ones that are thermal. This justifies step 1. in the above error mitigation scheme.

In order to ensure that the arbitrary threshold W_0 does not significantly affect the results we process the data using a range of different values. The peak associated with critical fluctuations remains relatively stable across this range (Fig. 7(a)). The same applies to the choice of W_f that enters in the definition of the interval. Large values close to W_0 result in a shift in the position of the peak with changing W_0 . This is unsurprising as any small change in the polarisation at finite B can push a given qubit below the threshold. This is not a reasonable criterion for identifying a dynamical damping. We therefore choose a more conservative value of $W_f/W_0 = 2/3$. Fig. 7(b) shows the number of qubits that enter the evaluation after all filters in the error mitigation scheme have been applied. We see that there is no significant drop until we reach a cutoff of $W \approx 0.48$. We therefore use $W_0 = 0.45$, corresponding to 35–45 qubits considered, to evaluate the data and extract the peak in critical fluctuations for different values of the Ising interactions strength J .

IV. CONCLUSION

We were able to simulate the time evolution of a spin chain under a Floquet unitary that produces time crystalline dynamics in a certain parameter regime. The transition to a non-DTC phase was observed via critical fluctuations in the amplitude of the sub-harmonic frequency response. The limitations of current NISQ devices allowed us to simulate relatively short time-scales only. We therefore used the unitary equivalence of this Floquet unitary to a random transverse field Ising Hamiltonian at even multiples of the driving period and the correspondence between DTC dynamics in the former and the breaking of a \mathbb{Z}_2 -symmetry in the latter to probe later times. We accounted for some of the gate errors introduced by trotterized time evolution on the quantum computer by factoring out an unphysical exponential decay and showed that the results are quite robust when varying the parameters that we were forced to introduce in the error mitigation scheme. We were able to reproduce the transition between the symmetry-broken and unbroken phases as indicated by critical fluctuations. A roughly linear scaling in the spin-spin interaction J of the transition point can be observed. These results are consistent with previous findings [10].

We conclude that the error rates on current NISQ devices do not allow us to make significant improvements on finite size effects and the MBL phase diagram. However, the DTC phase and the transition to a distinct MBL phase could be observed for a significantly larger system size, thus further substantiating the overall structure of the MBL phase diagram. With increasing fidelity of NISQ devices in the near-term future we can expect to shine light on some of the open problems in MBL, such as finite size scaling and the precise structure of the phase diagram.

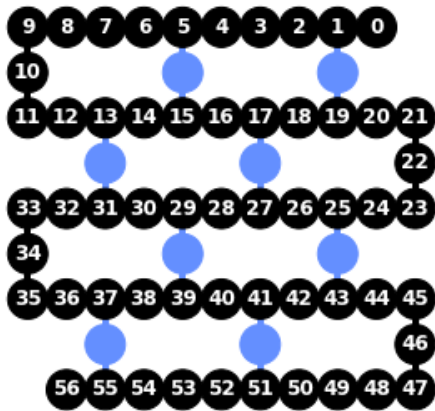


FIG. 8. Qubit layout on `ibmq_manhattan` chip with its 65 qubits (for which whole-device entanglement was demonstrated recently [50]). The 57 black qubits are used for the simulations of DTC.

Acknowledgements.— This work was supported by the University of Melbourne through the establishment of an IBM Quantum Hub at the University. SR acknowledges support from the Australian Research Council through Grants No. FT180100211.

-
- [1] Frank Wilczek. Quantum time crystals. *Physical Review Letters*, 109(16), Oct 2012.
- [2] Haruki Watanabe and Masaki Oshikawa. Absence of quantum time crystals. *Phys. Rev. Lett.*, 114:251603, Jun 2015.
- [3] Vedika Khemani, Roderich Moessner, and S. L. Sondhi. A brief history of time crystals, 2019.
- [4] Krzysztof Sacha and Jakub Zakrzewski. Time crystals: a review. *Reports on Progress in Physics*, 81(1):016401, nov 2017.
- [5] R. Moessner and S. L. Sondhi. Equilibration and order in quantum floquet matter. *Nature Physics*, 13(5):424–428, May 2017.
- [6] Soonwon Choi, Joonhee Choi, Renate Landig, Georg Kucsko, Hengyun Zhou, Junichi Isoya, Fedor Jelezko, Shinobu Onoda, Hitoshi Sumiya, Vedika Khemani, Curt von Keyserlingk, Norman Y. Yao, Eugene Demler, and Mikhail D. Lukin. Observation of discrete time-crystalline order in a disordered dipolar many-body system. *Nature*, 543(7644):221–225, Mar 2017.
- [7] Dominic V. Else, Bela Bauer, and Chetan Nayak. Floquet time crystals. *Phys. Rev. Lett.*, 117:090402, Aug 2016.
- [8] Wing Chi Yu, Jirawat Tangpanitanon, Alexander W. Glaetzle, Dieter Jaksch, and Dimitris G. Angelakis. Discrete time crystal in globally driven interacting quantum systems without disorder. *Phys. Rev. A*, 99:033618, Mar 2019.
- [9] J. Zhang, P. W. Hess, A. Kyprianidis, P. Becker, A. Lee, J. Smith, G. Pagano, I.-D. Potirniche, A. C. Potter, A. Vishwanath, N. Y. Yao, and C. Monroe. Observation of a discrete time crystal. *Nature*, 543(7644):217–220, Mar 2017.
- [10] N. Y. Yao, A. C. Potter, I.-D. Potirniche, and A. Vishwanath. Discrete time crystals: Rigidity, criticality, and realizations. *Phys. Rev. Lett.*, 118:030401, Jan 2017.
- [11] C. W. von Keyserlingk, Vedika Khemani, and S. L. Sondhi. Absolute stability and spatiotemporal long-range order in floquet systems. *Phys. Rev. B*, 94:085112, Aug 2016.
- [12] Arijeet Pal and David A. Huse. Many-body localization phase transition. *Phys. Rev. B*, 82:174411, Nov 2010.
- [13] I. V. Gornyi, A. D. Mirlin, and D. G. Polyakov. Interacting electrons in disordered wires: Anderson localization and low- t transport. *Phys. Rev. Lett.*, 95:206603, Nov 2005.
- [14] D. M. Basko, I. L. Aleiner, and B. L. Altshuler. Possible experimental manifestations of the many-body localization. *Phys. Rev. B*, 76:052203, Aug 2007.
- [15] Vadim Oganesyan and David A. Huse. Localization of interacting fermions at high temperature. *Phys. Rev. B*, 75:155111, Apr 2007.
- [16] Philipp Hauke and Markus Heyl. Many-body localization and quantum ergodicity in disordered long-range ising models. *Phys. Rev. B*, 92:134204, Oct 2015.
- [17] Elmer V. H. Doggen, Frank Schindler, Konstantin S. Tikhonov, Alexander D. Mirlin, Titus Neupert, Dmitry G. Polyakov, and Igor V. Gornyi. Many-body localization and delocalization in large quantum chains. *Phys. Rev. B*, 98:174202, Nov 2018.
- [18] David A. Huse, Rahul Nandkishore, Vadim Oganesyan, Arijeet Pal, and S. L. Sondhi. Localization-protected quantum order. *Phys. Rev. B*, 88:014206, Jul 2013.
- [19] J. Smith, A. Lee, P. Richerme, B. Neyenhuis, P. W. Hess, P. Hauke, M. Heyl, D. A. Huse, and C. Monroe. Many-body localization in a quantum simulator with programmable random disorder. *Nature Physics*, 12(10):907–911, Oct 2016.
- [20] Achilleas Lazarides, Arnab Das, and Roderich Moessner. Fate of many-body localization under periodic driving. *Phys. Rev. Lett.*, 115:030402, Jul 2015.
- [21] Pedro Ponte, Z. Papić, Fran çois Huveneers, and Dmitry A. Abanin. Many-body localization in periodically driven systems. *Phys. Rev. Lett.*, 114:140401, Apr 2015.
- [22] Jonas A. Kjäll, Jens H. Bardarson, and Frank Pollmann. Many-body localization in a disordered quantum ising chain. *Phys. Rev. Lett.*, 113:107204, Sep 2014.

- [23] David J. Luitz, Nicolas Laflorencie, and Fabien Alet. Many-body localization edge in the random-field heisenberg chain. *Phys. Rev. B*, 91:081103, Feb 2015.
- [24] Rahul Nandkishore and David A. Huse. Many-body localization and thermalization in quantum statistical mechanics. *Annual Review of Condensed Matter Physics*, 6(1):15–38, 2015.
- [25] Dmitry A. Abanin, Ehud Altman, Immanuel Bloch, and Maksym Serbyn. Colloquium: Many-body localization, thermalization, and entanglement. *Rev. Mod. Phys.*, 91:021001, May 2019.
- [26] Fabien Alet and Nicolas Laflorencie. Many-body localization: An introduction and selected topics. *Comptes Rendus Physique*, 19(6):498–525, 2018. Quantum simulation / Simulation quantique.
- [27] Ehud Altman and Ronen Vosk. Universal dynamics and renormalization in many-body-localized systems. *Annual Review of Condensed Matter Physics*, 6(1):383–409, 2015.
- [28] D.A. Abanin, J.H. Bardarson, G. De Tomasi, S. Gopalakrishnan, V. Khemani, S.A. Parameswaran, F. Pollmann, A.C. Potter, M. Serbyn, and R. Vasseur. Distinguishing localization from chaos: Challenges in finite-size systems. *Annals of Physics*, 427:168415, 2021.
- [29] Michael Schreiber, Sean S. Hodgman, Pranjal Bordia, Henrik P. Lüschen, Mark H. Fischer, Ronen Vosk, Ehud Altman, Ulrich Schneider, and Immanuel Bloch. Observation of many-body localization of interacting fermions in a quasirandom optical lattice. *Science*, 349(6250):842–845, 2015.
- [30] Jae-yoon Choi, Sebastian Hild, Johannes Zeiher, Peter Schauß, Antonio Rubio-Abadal, Tarik Yefsah, Vedika Khemani, David A. Huse, Immanuel Bloch, and Christian Gross. Exploring the many-body localization transition in two dimensions. *Science*, 352(6293):1547–1552, 2016.
- [31] G. Kucsko, S. Choi, J. Choi, P. C. Maurer, H. Zhou, R. Landig, H. Sumiya, S. Onoda, J. Isoya, F. Jelezko, E. Demler, N. Y. Yao, and M. D. Lukin. Critical thermalization of a disordered dipolar spin system in diamond. *Phys. Rev. Lett.*, 121:023601, Jul 2018.
- [32] Jared Rovny, Robert L. Blum, and Sean E. Barrett. Observation of discrete-time-crystal signatures in an ordered dipolar many-body system. *Phys. Rev. Lett.*, 120:180603, May 2018.
- [33] Marko Žnidarič, Antonello Scardicchio, and Vipin Kerala Varma. Diffusive and subdiffusive spin transport in the ergodic phase of a many-body localizable system. *Phys. Rev. Lett.*, 117:040601, Jul 2016.
- [34] Vedika Khemani, Frank Pollmann, and S. L. Sondhi. Obtaining highly excited eigenstates of many-body localized hamiltonians by the density matrix renormalization group approach. *Phys. Rev. Lett.*, 116:247204, Jun 2016.
- [35] Xiongjie Yu, David Pekker, and Bryan K. Clark. Finding matrix product state representations of highly excited eigenstates of many-body localized hamiltonians. *Phys. Rev. Lett.*, 118:017201, Jan 2017.
- [36] Thorsten B. Wahl, Arijeet Pal, and Steven H. Simon. Efficient representation of fully many-body localized systems using tensor networks. *Phys. Rev. X*, 7:021018, May 2017.
- [37] Elmer V. H. Doggen, Gabriel Lemarié, Sylvain Capponi, and Nicolas Laflorencie. Weak- versus strong-disorder superfluid—bose glass transition in one dimension. *Phys. Rev. B*, 96:180202, Nov 2017.
- [38] Suguru Endo, Simon C. Benjamin, and Ying Li. Practical quantum error mitigation for near-future applications. *Phys. Rev. X*, 8:031027, Jul 2018.
- [39] Adam Smith, M. S. Kim, Frank Pollmann, and Johannes Knolle. Simulating quantum many-body dynamics on a current digital quantum computer. *npj Quantum Information*, 5(1), Nov 2019.
- [40] Kishor Bharti, Alba Cervera-Lierta, Thi Ha Kyaw, Tobias Haug, Sumner Alperin-Lea, Abhinav Anand, Matthias Degroote, Hermanni Heimonen, Jakob S. Kottmann, Tim Menke, Wai-Keong Mok, Sukin Sim, Leong-Chuan Kwek, and Alán Aspuru-Guzik. Noisy intermediate-scale quantum (nisq) algorithms, 2021.
- [41] K. J. Satzinger *et al.* Realizing topologically ordered states on a quantum processor, 2021.
- [42] Frank Arute *et al.* Observation of separated dynamics of charge and spin in the fermi-hubbard model, 2020.
- [43] Dave Wecker, Matthew B. Hastings, Nathan Wiebe, Bryan K. Clark, Chetan Nayak, and Matthias Troyer. Solving strongly correlated electron models on a quantum computer. *Phys. Rev. A*, 92:062318, Dec 2015.
- [44] Adam Smith, Bernhard Jobst, Andrew G. Green, and Frank Pollmann. Crossing a topological phase transition with a quantum computer, 2020.
- [45] D. Zhu, S. Johri, N. H. Nguyen, C. Huerta Alderete, K. A. Landsman, N. M. Linke, C. Monroe, and A. Y. Matsuura. Probing many-body localization on a noisy quantum computer. *Phys. Rev. A*, 103:032606, Mar 2021.
- [46] Matteo Ippoliti, Kostyantyn Kechedzhi, Roderich Moessner, S. L. Sondhi, and Vedika Khemani. Many-body physics in the nisq era: quantum programming a discrete time crystal, 2021.
- [47] G.A.L. White, C.D. Hill, and L.C.L. Hollenberg. Performance optimization for drift-robust fidelity improvement of two-qubit gates. *Phys. Rev. Applied*, 15:014023, Jan 2021.
- [48] Harish J. Vallury, Michael A. Jones, Charles D. Hill, and Lloyd C. L. Hollenberg. Quantum computed moments correction to variational estimates. *Quantum*, 4:373, December 2020.
- [49] Joseph Vovrosh, Kiran E. Khosla, Sean Greenaway, Christopher Self, Myungshik Kim, and Johannes Knolle. Simple mitigation of global depolarizing errors in quantum simulations, 2021.
- [50] Gary J. Mooney, Gregory A. L. White, Charles D. Hill, and Lloyd C. L. Hollenberg. Whole-device entanglement in a 65-qubit superconducting quantum computer. arXiv:2102.11521.